MINISTRY OF EDUCATION AND TRAINING

VIETNAM ACADEMY OF SCIENCE AND TECHNOLOGY

GRADUATE UNIVERSITY OF SCIENCE AND TECHNOLOGY

Le Thi Quynh Xuan

RESEARCH ON COLD PLASMA TECHNOLOGY APPLIED IN SYNTHESIS OF NANO METAL MATERIALS, SEED TREATMENT AND DYES DECOMPOSITION

SUMMARY OF DISSERTATION ON MATERIAL SCIENCE

Major: Materials for Optics Optoelectronics and Photonics

Code: 9.44.01.27

Hanoi – 2025

The dissertation is completed at: Graduate University of Science and Technology, Vietnam Academy Science and Technology

Supervisors:

1. Dr. Dao Nguyen Thuan – Institute of Materials Science – Vietnam Academy of Science and Technology
2. Dr. Nguyen Van Chuc – Institute of Materials Science – Vietnam Academy of Science and Technology

Referee 1: .....

Referee 2: .....

Referee 3: .....

The dissertation is examined by Examination Board of Graduate University of Science and Technology, Vietnam Academy of Science and Technology at……..

The dissertation can be found at:

1. Graduate University of Science and Technology Library
2. National Library of Vietnam

Introduction

Cold plasma technology is emerging as a promising research field due to its wide applications in industry, medicine, agriculture, and environmental treatment. Thanks to its non-thermal nature, it can generate reactive species (ROS, RNS) without raising ambient temperature, making it suitable for sensitive materials and pollutant decomposition. Globally, cold plasma has shown effectiveness in seed germination, productivity improvement, and wastewater treatment. In Vietnam, its practical application remains limited, particularly in agriculture and pollution control.

This thesis presents research on using cold plasma in synthesizing nano-metals, seed treatment, and dye degradation. Chapter 3 discusses gold nanoparticle fabrication without chemical reducers; Chapter 4 focuses on surface treatment; and Chapter 5 explores seed germination stimulation and Methylene Blue decomposition. This approach addresses both agricultural productivity and environmental pollution, offering a cleaner, energy-efficient alternative to conventional methods.

Research objectives of the thesis:

- Making a cold plasma jet system with operating parameters such as voltage, frequency, irradiation distance and gas flow rate as a means of research for subsequent applications.
- Research on the application of cold plasm technology to synthesis gold nanoparticles with high uniformity with an average diameter of 45 nm, high purity and good stability in solution for a long time without using reducing chemicals or surface protection agents. The fabrication method needs to be evaluated, optimized and has high repeatability.
- Research on the fabrication of a SERS substrate with high sensitivity, stability and repeatability based on the substrate pretreatment with cold plasma technology. The fabrication method needs to be evaluated, optimized and has high repeatability.
- Research on stimulating seeds (mung bean) to germinate faster and more effectively by cold plasma treatment method. The treatment method needs to be evaluated, optimized and has high repeatability.
- Research on the treatment of dyes in wastewater (from dyeing factories) using cold plasma technology. The treatment method needs to be evaluated and optimized.

Research object:

- Gold nanoparticles have high homogeneity with an average diameter of 45 nm (absorption peak at nearly 532 nm), high purity and good stability in solution for a long time. These gold nanoparticles can be suitable for sensor applications based on the SERS effect, suitable for 532 nm laser excitation.
- SERS substrates made from gold metal nanoparticles have high sensitivity, stability and repeatability.

- Mung bean seeds have the ability to germinate.
- Methyl blue dye found in excess wastewater (from dye factories).

Research methods

This thesis employed experimental methods combined with measurement, calculation, and interaction analysis between cold plasma and treated objects. A high-voltage, high-frequency cold plasma jet system was built for treatment. Various modern techniques such as UV-VIS, OES, Raman, SEM, DLS, Zeta potential, XRD, NMR, and LC-MS were used to analyze gold nanoparticles and seed hormonal changes post-treatment. Additionally, methods like GA3 extraction, COD evaluation, and seed germination tests were applied to assess the effectiveness of plasma on seeds and Methylene Blue dye.

Thesis's structure and content

The thesis includes five chapters besides the introduction and conclusion:

- Chapter 1 gives an overview of cold plasma technology and its fundamental properties.
- Chapter 2 presents the chemicals, equipment, and methods used, detailing their principles and parameters.
- Chapters 3 to 5 cover experimental results on synthesizing gold nanoparticles, surface treatment for SERS substrates, seed germination stimulation, and dye degradation.

The thesis ends with a list of related publications and references.

New results of the thesis

This thesis, conducted at the Institute of Materials Science (VAST), achieved several key results:

1. Developed a cold plasma jet system with adjustable voltage (2–6 kV), frequency (100 Hz–80 kHz), distance (0.2–2 cm), and gas flow (3.4–10 scm) for research applications.
2. Synthesized uniform gold nanoparticles (~45 nm) without using reducing or protective agents, using optimized plasma conditions. The method is fast (5 mins), stable, and eco-friendly.
3. Fabricated high-performance SERS substrates, achieving 11× enhancement, 10 reuse cycles, LOD of 10^{-12} M (R6G), and successful amoxicillin detection with LOD of 9×10^{-10} M.
4. Enhanced seed germination: Plasma treatment increased germination coefficient 11-fold and seedling length nearly 3-fold. Plasma-induced NO regulated GA3 hormone levels, boosting growth.
5. Completely degraded Methyl Blue dye (30 ppm in 55 mins) using optimized plasma parameters, reducing COD to 42.52 mg/L, within national wastewater standards.

CHAPTER I:

OVERVIEW OF COLD PLASMA TECHNOLOGY

This chapter introduces plasma technology, classifies it into hot and cold plasma, and explains key physical parameters such as ionization degree and electron temperature. It further details cold plasma characteristics, generation methods at atmospheric pressure, and the formation of reactive species. The chapter concludes with an overview of cold plasma applications in materials, agriculture, and environment, illustrated by typical research examples and results.

CHAPTER II:

RESEARCH METHODS AND TECHNIQUES

This chapter details the experimental methods and techniques used throughout the thesis, including cold plasma systems, spectroscopy tools, and modern analytical instruments. It lists materials and advanced equipment (e.g. UV-VIS, OES, SEM, DLS, Zeta potential), and explains research methods such as Raman, NMR, LC-MS, and COD analysis. Each technique is described with its principles and parameters, ensuring data reliability and reproducibility.

CHAPTER III:

COLD PLASMA TECHNOLOGY APPLIED IN SYNTHESIS OF METAL NANOPARTICLES

3.1. Concept and properties of metal nanomaterials

3.2. Methods of manufacturing gold nanoparticles

3.3. Research on manufacturing gold nanoparticles using plasma jet method

3.3.1. General diagram of manufacturing steps

The research group initially discussed and proposed the basic steps of an experiment to fabricate Au nanoparticles using the plasma jet method (Figure 3.1) and the detailed steps are described in Figure 3.1

Figure 3.2 illustrates the plasma jet system for AuNP synthesis, powered by a high-voltage (2–6 kV), high-frequency (100 Hz–80 kHz) source. The setup includes a quartz tube housing a stainless-steel needle (high-voltage electrode) and a copper tape (ground electrode).

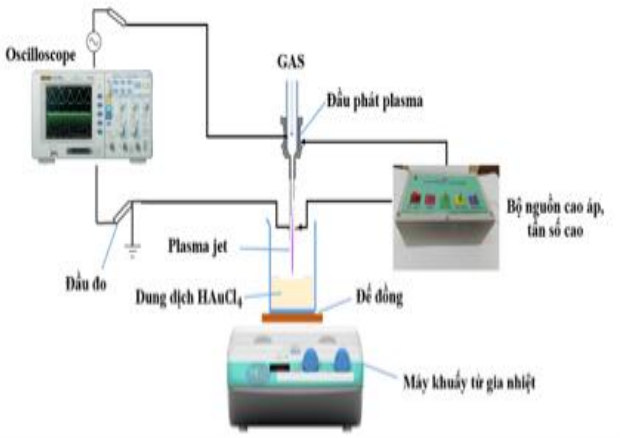

Figure 3.2. *Schematic diagram of the experimental synthesis of Au nanoparticles using plasma jet system.*

3.3.2. Effect of distance from plasma tip to solution surface

Photographs of AuNPs samples with different distances d: (A) 0.2 cm, (B) 0.3 cm and (C) 0.4 cm are shown in Figure 3.3

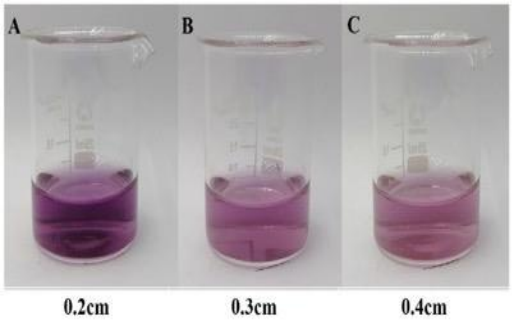

***Figure 3.3**. Photographs of AuNPs samples with different d-spacings: (A) 0.2 cm, (B) 0.3 cm, and (C) 0.4 cm.*

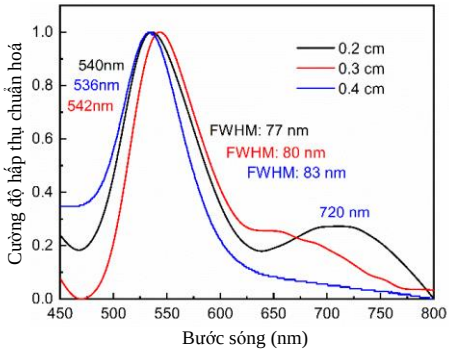

***Figure 3.4**. Normalized absorption spectra of AuNPs samples with different d-spacings.*

Figure 3.4 shows the normalized absorption spectrum dependence of AuNPs synthesized at different distances (d) from the quartz tip to the liquid surface. From the color and absorption spectra of the three samples obtained, the peaks of all three samples are almost identical and are near ~ 535 nm. The half-width (FWHM) of the sample with a distance of d = 0.4 cm gives the narrowest value.

3.3.3. Effect of distance from plasma generator to solution surface

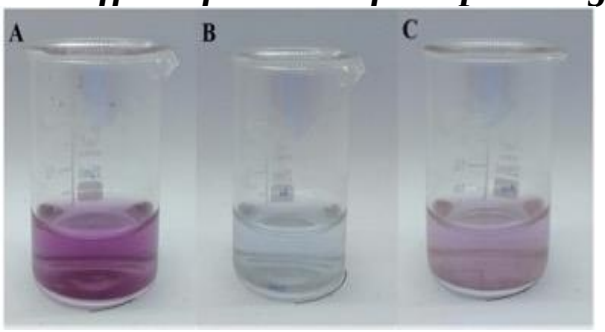

***Figure 3.5**. AuNPs samples with different gas flow rates.*

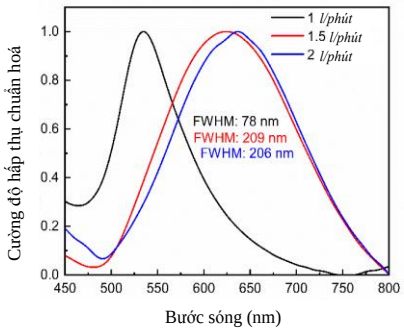

***Figure 3.6**. UV-Vis spectra of AuNPs samples with different gas flows*

Figure 3.6 shows the normalized absorption spectra of AuNPs synthesized with different gas flow rates precisely controlled by the gas flow control valve. The gas flow rate of 1 l/min is the optimal condition leading to the narrowest absorption spectrum (FWHM = 75 nm). With higher gas flow rates (1.5 – 2 l/min), the reaction rate is much faster and more particles of different sizes can be produced during the plasma reaction, leading to a very broad absorption spectrum (FWHM > 200 nm).

3.3.4. Effect of plasma source frequency

The images of the samples captured in Figure 3.7 show the different densities of the solutions synthesized at different frequency conditions. The normalized absorption spectra and the half-width of each sample are shown in Figure 3.8. At 40 kHz, we

obtained the most homogeneous AuNPs with an absorption spectrum peaking at 535 nm and the narrowest half-width (FWHM = 80 nm).

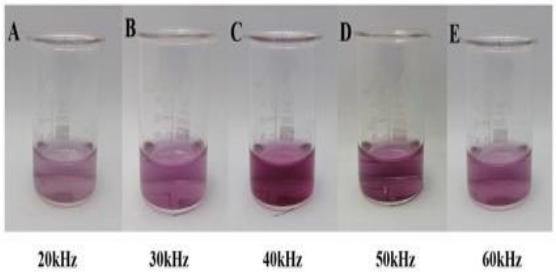

Figure 3.7. *Photographs of AuNPs samples with different plasma frequency*

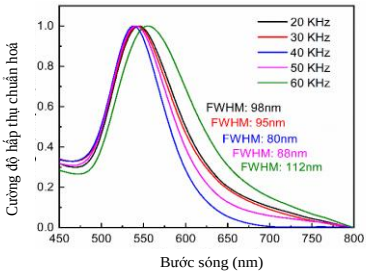

Figure 3.8. *Normalized absorption spectra of AuNPs samples with different plasma frequencies.*

3.3.5. Effect of synthesis time

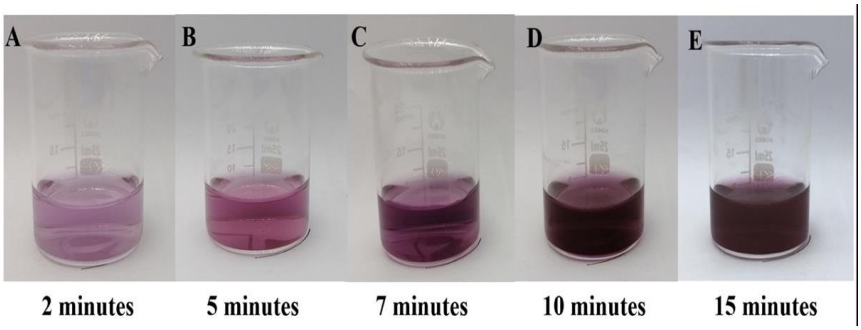

Figure 3.9. *AuNps samples synthesized by Plasma jet with different times: (A) 2 minutes; (B) 5 minutes; (C) 7 minutes; (D) 10 minutes and (E) 15 minutes.*

Accordingly, we conducted the experiment with 5 different times as shown in Figure 3.9. When conducting the experiment, we fixed the parameters of the plasma jet source at 10V voltage and 40kHz frequency

We propose the explanation that when the irradiation time is more than 5 minutes, the generated particles continue to collide and merge with each other (due to the lack of surface protection and the rotational force of the magnetic stirrer), thereby forming larger particle sizes than those generated mainly at the irradiation time of 5 minutes (shown in Figure 3.10).

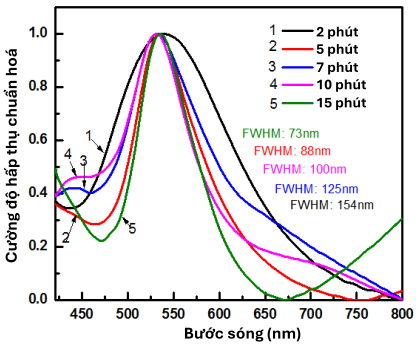

Figure 3.10*. Normalized absorption spectra of AuNps samples synthesized by plasma jet with different times*

3.3.6. Effect of precursor solution concentration $HAuCl_4$

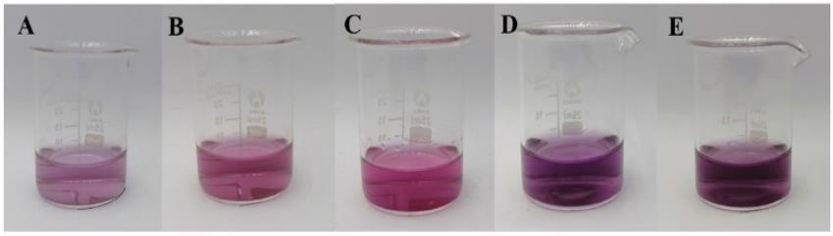

Figure 3.11. *Photographs of AuNPs samples with different precursor concentrations*

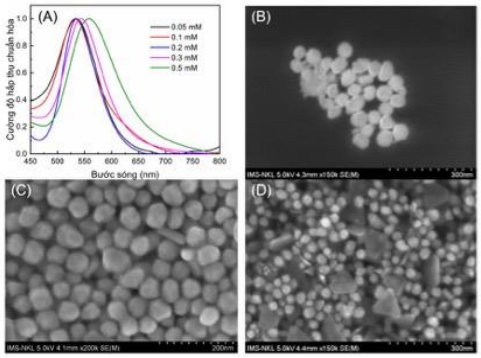

Figure 3.12. *(A) Normalized absorption spectra of AuNPs samples with different precursor concentrations, (B)-(D) SEM images of AuNPs samples with precursor concentrations (B) 0.05 mM, (C) 0.2 mM and (D) 0.5 mM.*

Thus, from the absorption spectrum analysis results, the precursor concentration of 0.2 mM was determined to be optimal for the synthesis of Au with uniform size and high particle number. To verify this conclusion, we conducted SEM imaging of samples with concentrations of 0.05 mM, 0.2 mM and 0.5 mM (Figure 3.12B-D). The 0.2 mM sample (Figure 3.12C) showed particles with uniform size (about 50 nm), evenly distributed in the solution, without any agglomeration or clustering.

3.3.7. Effect of $HAuCl_4$ precursor solution volume

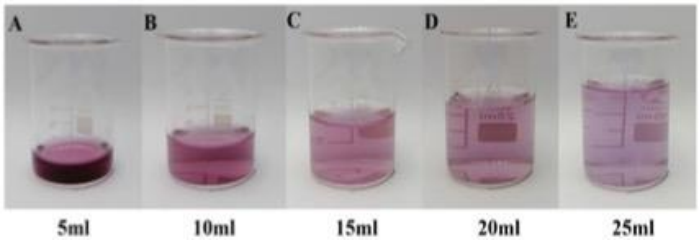

Figure 3.13. *Photographs of AuNPs with different volumes of precursor solutions.*

To study this effect, our group conducted experiments to fabricate AuNPs on different precursor solution volumes as shown in Figure 3.13. All samples had a precursor solution concentration of 0.2 mM and were irradiated with plasma for 5 minutes with a plasma source at 10V and a frequency of 40kHz. After the experiment was completed, all samples were analyzed for absorption spectra (Figure 3.14) to draw conclusions.

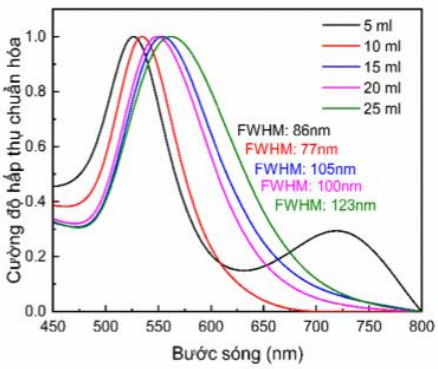

Figure 3.14. *Normalized absorption spectra of AuNPs samples with different volumes of precursor solutions.*

3.4. Properties and reaction mechanism of AuNPs synthesis by cold plasma jet

3.4.1. Optimal conditions for synthesis of AuNPs solution by plasma

We have come up with the following optimal parameters: Distance from plasma generator to liquid surface: 0.4 cm; Air flow rate: 1 l/min; Frequency of power supply for plasma generation: 40 kHz; Volume and concentration of HAuCl4 solution are 10 ml and 0.2 mM, respectively; Plasma irradiation time: 5 min.

3.4.2. Evaluation of the properties of the synthesized gold nanoparticles

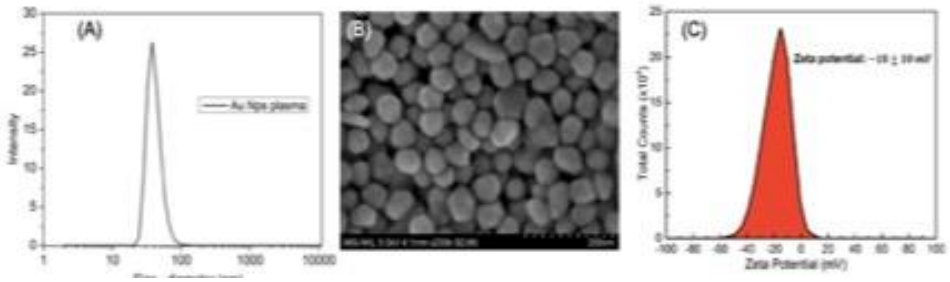

Figure 3.15*. (A) Particle size distribution by DLS method, (B) SEM image and (C) zeta potential of AuNPs synthesized under optimized conditions*

The results show that the AuNPs particles are mainly polygonal in shape instead of ideal spherical, with relatively uniform size and shape. Figure 3.15B illustrates the SEM image of AuNPs synthesized under optimal conditions.

The average diameter of the particles was determined to be approximately 45 nm, consistent with the results measured by DLS (Figure 3.15A), in which the particle size ranged from 20 - 110 nm, with an average diameter of 45 ± 15 nm. Figure 3.15C shows that the Zeta potential -18 ± 10 mV.

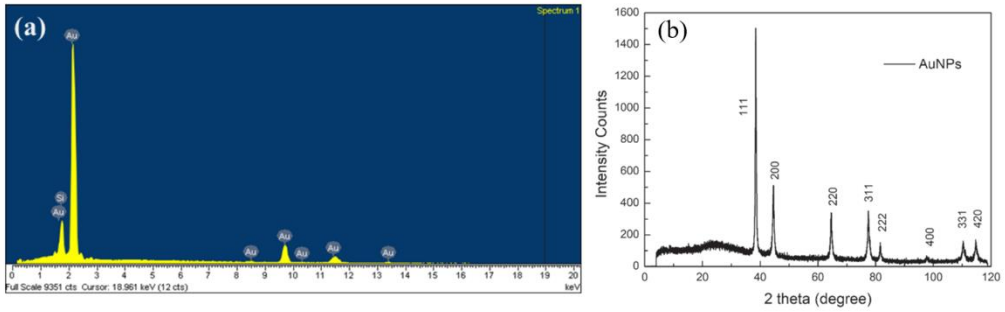

Figure 3.16. (A) EDX spectrum and (B) XRD spectrum of AuNPs.

Figure 3.16 shows the X-ray diffraction (XRD) and EDX spectra, confirming the crystal structure of the synthesized AuNPs. This proves that the synthesized

3.4.3. Study of the reaction mechanism of AuNPs synthesis by cold plasma

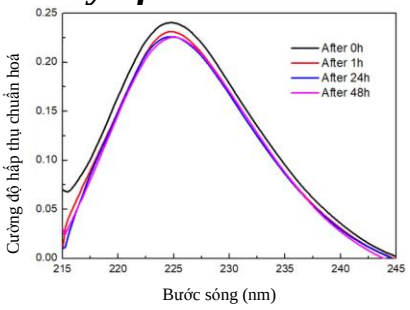

Figure 3.17. *Changes in the absorption spectrum of H2O2 in plasma-treated water for 5 min after 0-48 h.*

In the liquid plasma system, where the electrodes are directly immersed in the solution, hydrogen radicals (H) are abundantly produced through water electrolysis, which play an important role in the reduction of gold ions. In the Plasma method of AuNPs synthesis, the reduction reaction of Au3+ mainly relies on H2O2 and OH-, as described in the following equation:

$$3H_2O_2 + 3OH^- + Au^{3+} \rightarrow Au^0 + 3H_2O + 3HO_2$$

3.5. Application of fabricated gold nanoparticles to develop highly sensitive SERS substrates

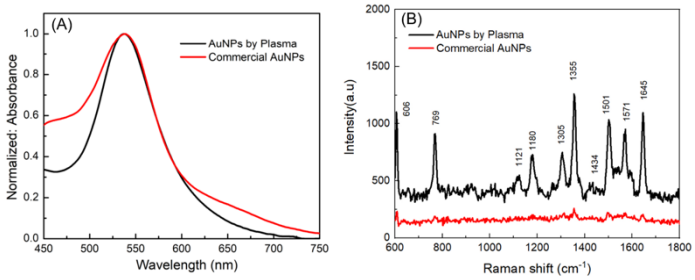

Figure 3.18. *Comparison of (A) Normalized absorption spectrum and (B) Raman spectrum of AuNPs synthesized by plasma method and commercial AuNPs at 100b R6G solution*

The SERS intensity of substrates using plasma-synthesized AuNPs was significantly higher than that of substrates using commercial AuNPs. We also emphasize that the SERS intensity is highly dependent on the experimental conditions. Therefore, the lower SERS signal observed with commercial AuNPs in this study cannot be directly compared with results from other studies

3.6. Conclusion of chapter 3

This chapter reviews cold plasma applications in synthesizing metal nanoparticles, especially AuNPs. It outlines nanomaterial concepts, fabrication methods, and highlights cold plasma as a green synthesis technique. A systematic study optimized plasma parameters (e.g., 0.4 cm nozzle distance, 1 L/min gas flow, 40 kHz frequency) to produce uniform 45 nm AuNPs without reducing agents. Analytical methods (SEM, XRD, UV-Vis, DLS) confirmed stability and size uniformity. The plasma-synthesized AuNPs showed superior SERS enhancement over commercial ones, indicating strong potential for biosensor, biomedical, and catalytic applications. The results of the research in this chapter have been published in the journal Nanotechnology (IF 2.9).

CHAPTER IV:

COLD PLASMA TECHNOLOGY APPLIED IN MANUFACTURING SERS BASES FOR DEVELOPMENT OF BIOCHEMICAL SENSORS

The main objective of this research is to study the application of cold plasma technology in the surface treatment of materials used in the development of biochemical sensors based on the SERS effect. This report presents two main contents: (1) Research on the application of cold plasma technology in the surface treatment of polycarbonate and SiO2 materials and (2) Research on the application of cold plasma technology in the development of biochemical sensors based on the SERS effect.

4.1. Research on the application of cold plasma technology in the surface treatment of polycarbonate and SiO2 materials

4.1.1. Process of applying cold plasma technology in the surface treatment of materials

4.1.1.1. Polycarbonate (PC) materials

In this research, we mainly study and optimize the surface energy enhancement effect of PC by plasma treatment, which allows to enhance the bonding of different coatings on the PC surface.

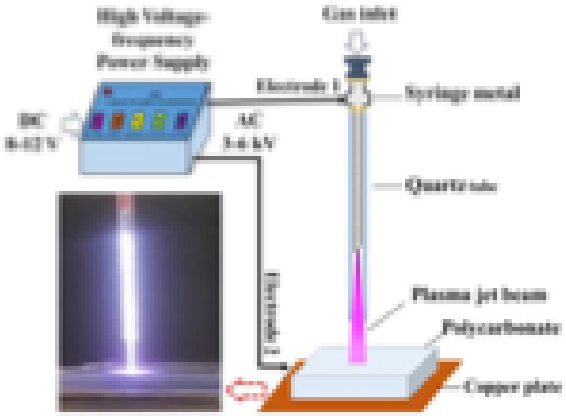

Figure 4.1. *Schematic diagram of plasma jet system for PC surface treatment and photo taken during plasma treatment.*

Figure 4.1 shows the schematic diagram of the plasma jet system used in material surface treatment, which consists of two main components: (1) high-voltage, high-frequency power source, and (2) plasma generator. The effect of plasma surface treatment on PC samples is calculated according to the following equation:

$$H = \frac{WAC_{not\ treatment} - WAC_{treated}}{WAC_{not\ treatment}}$$

4.1.1.2. SiO_2 material

In this study, we applied cold plasma technology to the surface of a glass substrate (SiO_2) by irradiating a plasma jet beam onto the entire surface bounded by polyimide tape. The steps for treating the surface of SiO_2 material are similar to those for treating the surface of PC material.

4.1.2. Survey, evaluate the effectiveness and duration of the surface treatment effect of materials using plasma jet method

4.1.1.1. On polycarbonate materials

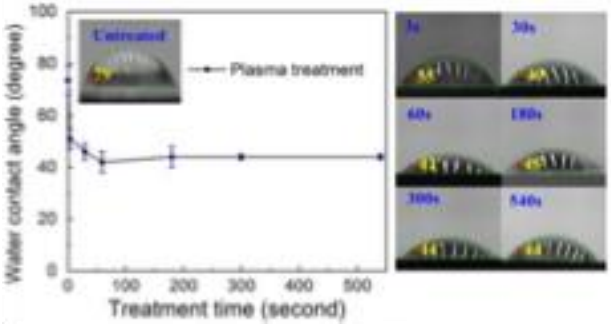

Figure 4.2. *(Left): dependence of water contact angle (WCA) on PC surface on plasma treatment time; (right): photographs of water droplets on PC surface at different plasma treatment times.*

This study varied plasma irradiation time to observe surface changes on PC materials via water contact angle (WCA) measurements. Higher plasma-induced surface energy led to greater WCA reduction. Over 14 days, WCA change dropped from ~40% to <10% for short treatments (3–60 s), demonstrating long-term surface effects. These effects support enhanced coatings (anti-fog, anti-scratch, antibacterial, etc.), broadening PC's application potential.

The plasma-induced PC surface modification is clearly observed through the atomic force microscopy (AFM) image in Figure 4.4.

Plasma surface treatment induces both chemical (surface energy, bonding) and physical (microcracks) changes. Surface energy changes occur within the first 3–60 seconds and fade over 7 days due to environmental exposure. However, longer plasma durations (≥180 s) result in more persistent effects on water contact angle (WCA), with physical changes maintaining 20% impact even after 14 days.

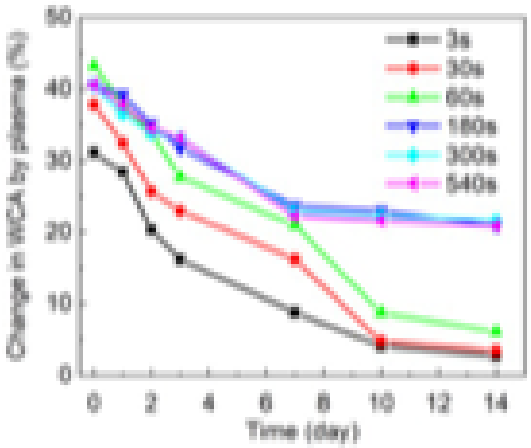

Figure 4.3. *Long-term effects obtained for different plasma irradiation times (3 s, 30 s, 60 s, 180 s, 300 s, 540 s) on PC surface from immediately to after 140 days.*

AFM images reveal plasma-induced surface changes on PC. The increase in oxygen-containing polar groups raises surface energy and hydrophilicity, lowering contact angle. However, excessive plasma exposure saturates the O:C ratio, limiting contact angle reduction (to 42° in this study).

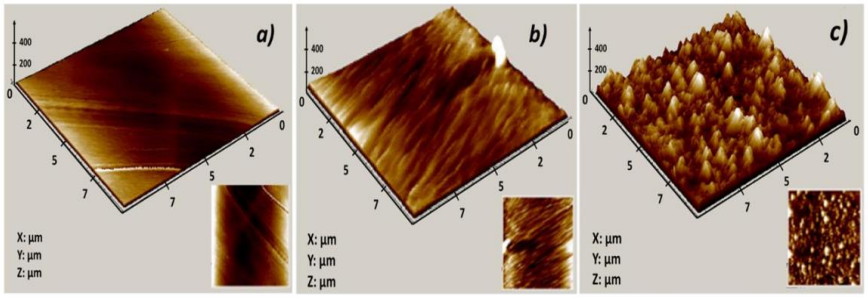

Figure 4.4. *AFM images of PC surface: a) without plasma treatment, b) plasma treatment for 60 s and c) plasma treatment for 540 s*

4.1.1.2. On SiO_2 material

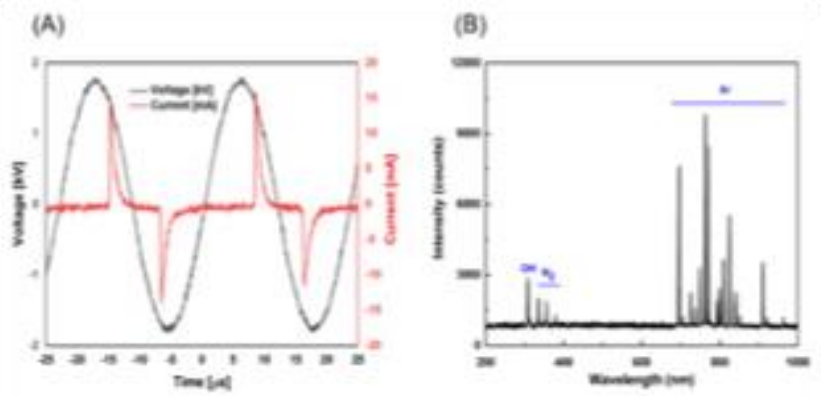

Figure 4.5*. (A) I-V diagram and (B) Optical emission spectrum of the plasma jet system.*

Plasma jet properties were evaluated via I–V and OES analysis. Plasma treatment reduced glass surface roughness (from 200 nm to nearly smooth after 30 s) and decreased water

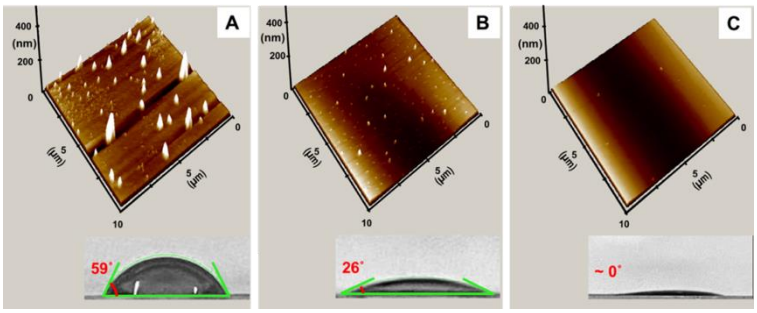

Figure 4.6. *AFM images of the glass surface and water contact angle (WCA) images (bottom right: (C) before, (D) after 10 s, and (E) after 30 s of plasma treatment*

contact angle (from 59° to near 0°), enhancing surface energy. These effects improve AuNP adhesion during SERS substrate fabrication.

Similar to PC material, we mainly varied the plasma irradiation time to investigate the effect of plasma on changes on the glass substrate surface through changes in surface structure and monitoring changes in water contact angle (WCA). It investigate the factors that can cause changes in the surface of the glass substrate material, we tested the plasma properties of the plasma jet generation system by measuring the current-voltage (I-V) characteristics and analyzing the optical emission spectrum (OES) of the system (Figure 4.5). Figure 4.6A-C shows the effects of different plasma treatment times on the glass surface

4.2. Research on the application of cold plasma technology in the development of biochemical sensors based on the SERS effect

In this study, we and our research team combined cold plasma and laser methods to develop a simple, low-cost, yet effective method for rapid and high-performance fabrication of SERS substrates. Accordingly, the first step was to fabricate Au nanoparticles (AuNPs) by plasma technology from $HAuCl_4$ precursor with the process described in detail in research content 3 for use as SERS substrates.

4.2.1. Processing in SERS substrate using plasma jet technology

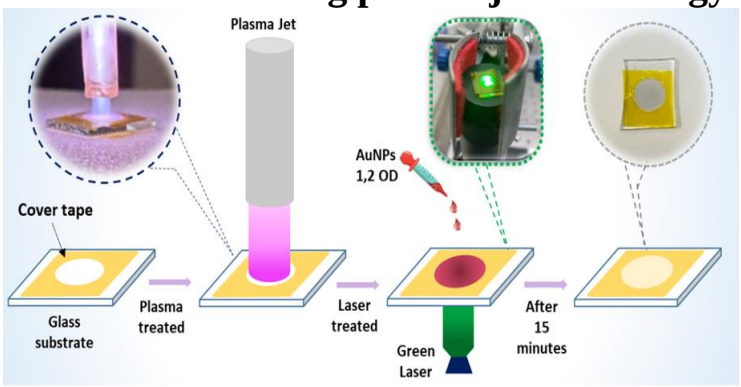

Figure 4.7. *Fabrication process of SERS substrate combining plasma pretreatment and laser treatment*

Figure 4.7 illustrates the SERS substrate fabrication process combining cold plasma and laser techniques using plasma-synthesized AuNPs. Steps include: (1) preparing glass substrates, (2) 30 s plasma treatment to clean and functionalize the surface, (3)

dropping 3 µl of AuNP solution, and (4) 15 min blue laser (532 nm, 480 mW) irradiation to deposit AuNPs.

4.2.2. Investigation and evaluation of the effectiveness of the fabricated SERS substrate

4.2.2.1. Enhanced intensity and uniformity of Raman signal over a large area

To evaluate the effect of cold plasma pretreatment and laser treatment on SERS substrates, we compared the Raman spectra of R6G on different SERS substrates: substrates fabricated without any surface treatment (black line), substrates treated with plasma but not laser (purple line), and treated with both laser and plasma (green line). We demonstrated that the combination of plasma and laser improved the surface quality and produced a more uniform distribution of AuNPs on the substrate, resulting in enhanced Raman intensity and a more uniform SERS substrate, thus, more consistent SERS signals (Figure 4.8).

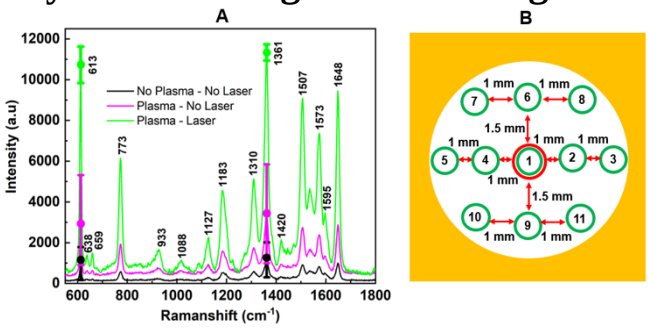

Figure 4.8. *(A) Raman spectra of R6G measured on SERS substrates fabricated without plasma or laser pretreatment (black line), pretreated with cold plasma only (purple line), and treated with both cold plasma and laser (blue line). Each Raman spectrum is the average of 11 measurements at 11 different points distributed over the entire substrate surface (B), and their deviations are shown by error bars on the characteristic peaks at 613 cm^{-1} and 1361 cm^{-1}*

4.2.2.2. Improved reusability of SERS substrates

SERS substrate reusability was tested using 10^{-6} M R6G, followed by cleaning and re-adsorption over 10 cycles.

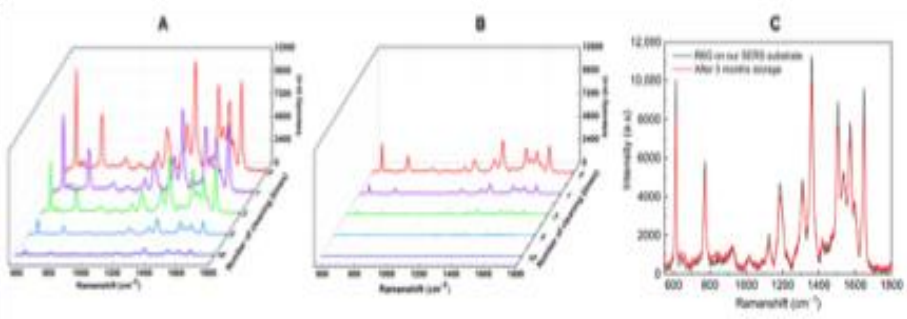

Figure 4.9. *Raman spectra of R6G after washing the substrate 0, 1, 3, 5 and 10 times for cold plasma and laser pretreatment (A) compared to cold plasma pretreatment only (B); (C) Raman intensity of R6G on the fabricated SERS substrate before and after 3 months at room temperature*

Raman spectra confirmed no residual R6G and stable signal retention. Substrates treated with plasma + laser maintained clear signals after 10 uses, while plasma-only substrates showed weak signals after 5 cycles.

Furthermore, we observed that the Raman intensity of R6G on the fabricated SERS substrate remained at 85% after 3 months of storage at room temperature (Fig.

4.9C). This demonstrates the stability, reusability, and cost-effectiveness of our (plasma + laser) treated SERS substrate.

4.2.2.3. SERS enhancement factor (EF) and sensitivity to R6G

The uniform distribution of AuNPs on the surface from plasma and laser treatments, our SERS substrate achieved a remarkable EF of $3.2.10^8$.

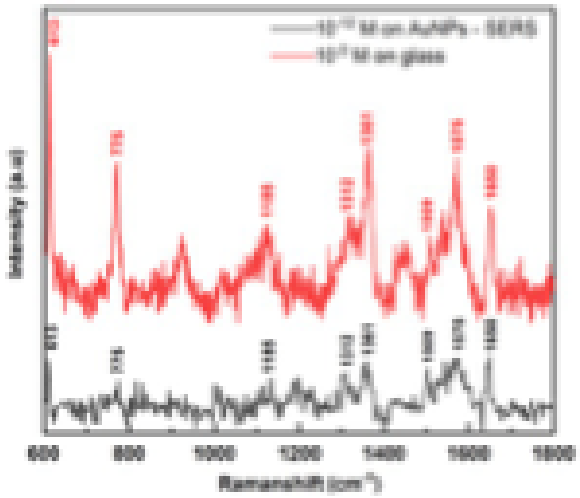

Hình 4.1. *Raman spectra of R6G after 0, 1, 3, 5, and 10 washing cycles on substrates treated with cold plasma and laser (A) compared to cold plasma treatment only (B); (C) Raman intensity of R6G on fabricated SERS substrates before and after 3 months at room temperature.*

Raman signal enhancement, R6G was used as a standard Raman reagent. Simplified, the enhancement factor (EF) is calculated as follows:

$$EF_{SERS} = \frac{I_{SERS}}{I_R} . \frac{C_R}{C_{SERS}}$$

C_R và C_{SERS} là concentration of R6G at the normal substrate (normal Raman) and the SERS, and IR and ISERS measurements are their peak intensities, respectively. Figure 4.10 shows the SERS spectrum of R6G at an ultra-low concentration of 10^{-12} M, measured on the fabricated SERS substrate. Using the Raman signal of R6G at 10^{-12} M on the SERS substrate and 10^{-3} M on the glass substrate, we calculated the enhancement factor:

$$EF_{SERS} = \frac{I_{SERS}}{I_R} . \frac{C_R}{C_{SERS}} = \frac{217}{667} . \frac{10^{-3}}{10^8} = 3{,}2 \, . \, 10^8$$

4.3. Testing of the fabricated SERS substrate for the detection of antibiotic Amoxicillin with high sensitivity

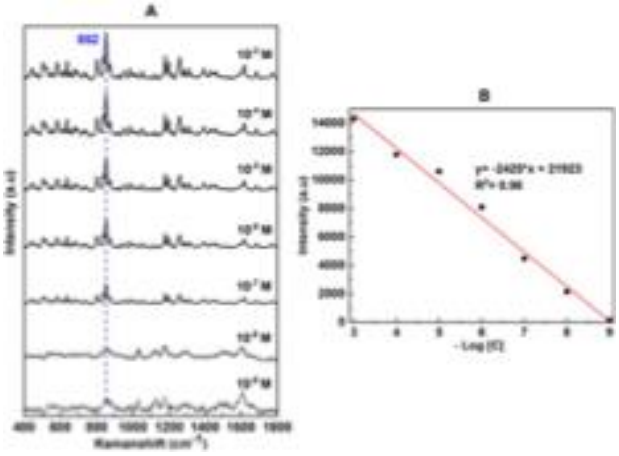

Figure 4.11. *SERS spectrum of Amoxicillin at different concentrations (A) and linear fit between its concentration and peak intensity at 852*

The fabricated SERS substrate was used to detect amoxicillin—a widely used antibiotic with potential health risks. SERS spectra (10^{-3} to 10^{-9} M) showed characteristic peaks at 1456, 1276, and 852 cm^{-1}. The method demonstrated high reliability with an R^2 value of 0.98. Using the Raman signal of Amoxicillin at 10^{-6} M on SERS substrate and 1 M on glass substrate, we calculated the enhancement factor and the Limit of Detection (LOD) was determined to be 0.9 x 10^{-9}:

cm-1 (B) over the concentration range from 10^{-3} to 10^{-9} M.

$$EF_{SERS} = \frac{I_{SERS}}{I_R} . \frac{C_R}{C_{SERS}} = \frac{161}{1887} . \frac{1}{10^{-9}} = 8{,}5 . 10^7$$

4.4. Chapter 4 Conclusion

This chapter presents the application of cold plasma in surface treatment for SERS-based biosensor development. Plasma treatment improved surface energy, hydrophilicity (WCA), and texture (AFM), with 60 s being optimal. Cold plasma pretreatment on SiO_2 enhanced SERS substrate performance. Combining plasma and laser enabled uniform AuNP deposition, achieving 11× Raman intensity, 10-time reuse, EF ~3×10^8 , and LOD of 10^{-12} M (R6G) and 9×10^{-10} M (amoxicillin, $R^2 = 0.98$). These results highlight cold plasma as a powerful tool for fabricating sensitive, high-precision biochemical sensors.The research results in this chapter have been published in the journals Nanomaterials (IF 4.4), Optical Materials (IF 3.8), and Vietnam Journal of Catalysis and Adsorption.

CHAPTER V:
COLD PLASMA TECHNOLOGY APPLIED IN STIMULATING SEED GERMINATION AND DYE DECOMPOSITION

5.1. Tests and steps of applying cold plasma technology in stimulating seed germination

5.1.1. Effects of cold plasma on the surface of

Cold plasma treatment improves both surface properties and internal composition of seeds. It enhances surface wettability by reducing surface energy, as indicated by decreased water contact angle.

5.1.2. Effect of cold plasma on seed germination

Cold plasma enhances seed germination by accelerating sprouting, increasing germination rate, and breaking dormancy. Its effects vary by gas type and exposure time, with short treatments improving seed viability and growth through enhanced surface hydrophilicity and antioxidant enzyme activation.

5.1.3. Effects of plasma on seedling growth

The early growth of seedlings is closely linked to the germination process, and the use of cold plasma or plasma activated water (PAW) has been shown to provide significant improvements.

5.1.4. Processing of application cold plasma technology in seed treatment

This process includes 7 main steps. In the plasma jet seed treatment process, ensure each step is carried out systematically to achieve optimal efficiency in stimulating seed germination and growth.

5.2. Survey and evaluation of seed germination efficiency after plasma treatment

We investigated the effect of cold plasma on bean sprout germination using a plasma jet (5 kV, 40 kHz, 400 sccm) with a 5 cm seed distance. Uniform seeds were selected, treated in batches of 25, and incubated at 28 °C with 5 ml water added every 12 hours to maintain stable growth conditions.

5.2.1. Germination coefficient

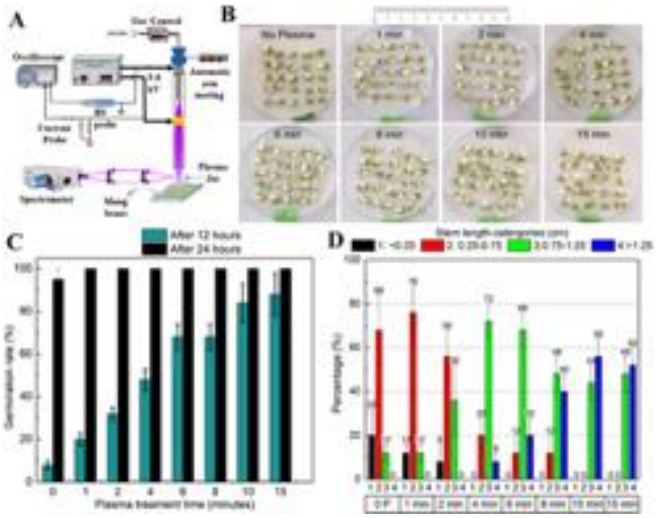

Figure 5.1. *(A) Schematic diagram of the plasma jet system for treating bean seeds. (B) Photographs of seeds after 24 hours and (C) Germination coefficients with different plasma treatment times. (D) Effect of plasma treatment time on root length at the germination stage. The error column is calculated from 5 different measurements (total of 125 seeds with each plasma treatment time).*

The germination and root development of bean sprouts were significantly improved after cold plasma treatment (Figure 5.1B). After 12 hours of incubation on cotton fabric, the germination coefficient (defined as the percentage of germinated seeds to the total number of seeds) increased from 8% to 88% (11-fold increase) when the seeds were plasma treated for 15 minutes, compared to the group of seeds that were not treated with plasma (Figure 5.1C).

5.2.2. Length of young roots immediately after

After 24 hours, plasma-treated seeds showed significantly greater root lengths. While 70% of untreated seeds had roots 0.25–0.75 cm, 70% of 4-min treated seeds reached 0.75–1.25 cm, and 60% of 10-min treated seeds exceeded 1.25 cm. The optimal condition was 10 min irradiation at 1.2 W (0.08 Wh/seed).

5.3. Mechanism of physical and biochemical changes induced by plasma treatment

5.3.1. Physical changes on the particle surface after plasma

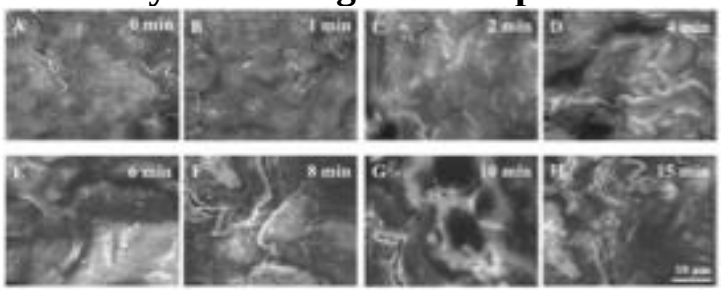

Figure 5.2. *SEM images of bean seed surface before plasma treatment (A) 0 min, and after plasma treatment after (B) 1 min, (C) 2 min, (D) 4 min, (E) 6 min, (F) 8 min,*

After plasma treatment, we investigated the changes on the seed coat surface (in this study, green bean and black bean seeds). The results showed that plasma treatment produced a clear transition from a partially wetted surface state to an almost completely wetted surface state when comparing untreated seeds

(G) 10 min and (H) 15 min.

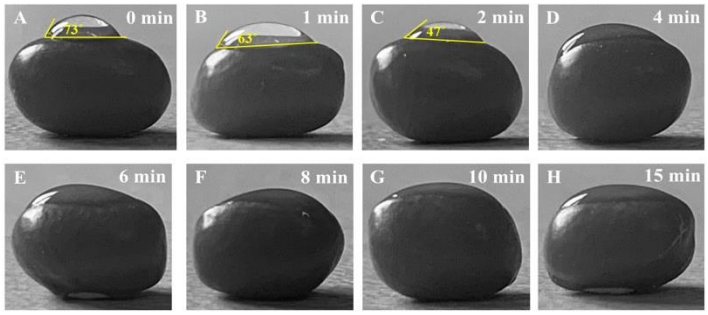

Figure 5.2. *SEM images of bean seed surface before plasma treatment (A) 0 min, and after plasma treatment after (B) 1 min, (C) 2 min, (D) 4 min, (E) 6 min, (F) 8 min, (G) 10 min and (H) 15 min.*

and seeds treated with plasma jet. The improvement in wettability, together with the formation of µm-sized cracks, is directly proportional to the plasma irradiation time. These changes increase the water absorption capacity on the seed surface, contributing to faster germination and seed growth. The WAC value gradually decreases with increasing plasma irradiation time.

5.3.2. Biochemical changes of seeds after plasma treatment

While surface changes increased with longer plasma exposure, 10 minutes gave optimal germination, indicating effects beyond physical modification—specifically hormonal regulation. To explore this, the ROS/RNS ratio was adjusted by varying plasma tube length.

5.3.2.1. Effect of plasma generator length on RONS ratio

Adjusting plasma tube length allowed better control of ROS/RNS ratios compared to DBD or sliding arc systems. Fluorescence spectra showed distinct N_2 (337 nm) and ●OH (309 nm) peaks across tube designs. GA_3 levels in mung beans were analyzed pre/post-treatment using LC-MS to assess hormonal regulation effects.

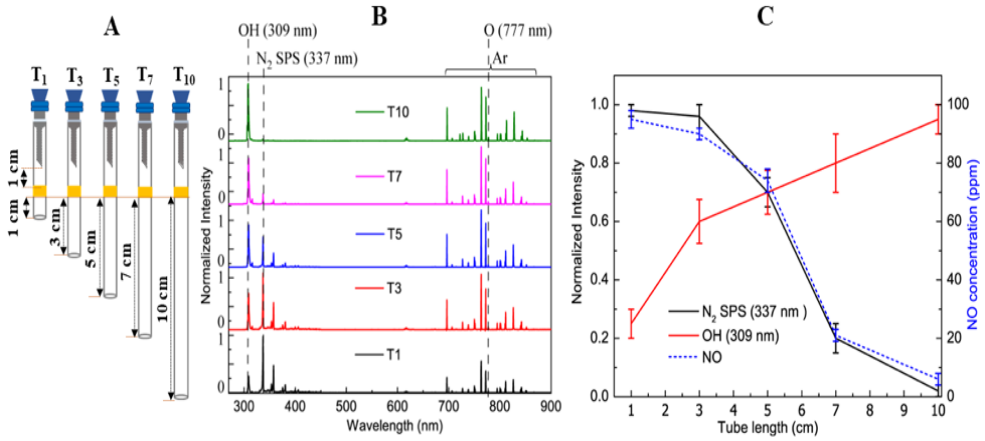

Figure 5.4. *(A) Different plasma tube lengths that we have fabricated. (B) Fluorescence spectra of the plasma in the range of 270–900 nm. (C) Dependence of fluorescence intensity of N2 SPS (337 nm), OH radical (309 nm) and NO concentration on different plasma tube lengths.*

5.3.2.2. Effect of RONS on the regulation of natural growth hormone

During the extraction process with black beans, the color from the seed coat dissolved into the extraction solution, affecting the analysis results. Therefore, we only conducted chemical analyses on the extracted samples from mung beans. These results indicate that the regulation of GA3 content, stimulated by the NO

concentration in the plasma, is the biochemical mechanism leading to the effect of promoting seed germination and growth.

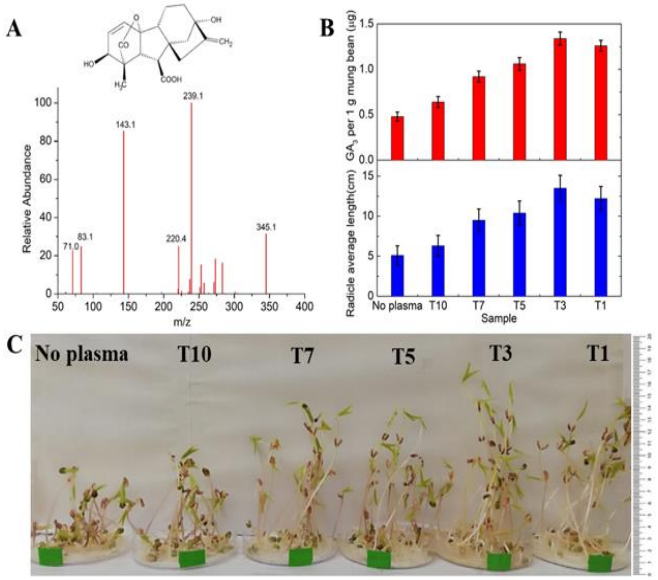

Figure 5.1. *(A) Mass spectrum of the extracted solution and chemical structure of gibberellic acid (GA3). (B) GA3 content (μg) in 1 g of bean seeds (red, top) and average shoot length (blue, bottom) as a function of plasma tube length. (C) Photographs of bean plant samples after 96 h.*

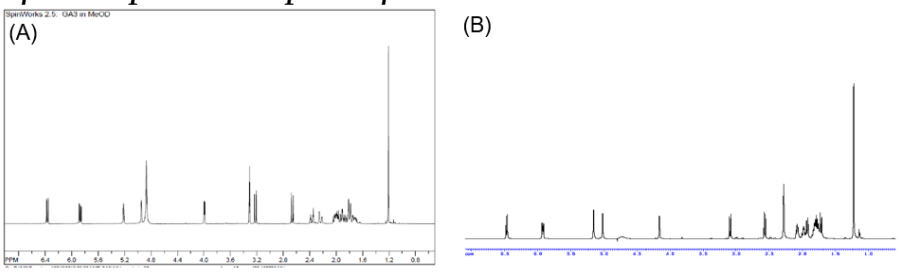

Figure 5.6. *NMR spectrum of gibberellic acid (GA3) from the extracted sample and comparison with the spectrum of the standard sample.*

An optimal NO concentration of 20–95 ppm (tube length 1–7 cm) was recommended, as excess NO may disrupt GA_3 regulation. A larger sample mass was used for extraction, and NMR confirmed the extracted compound as gibberellic acid (GA_3).

5.4. Tests and application steps of cold plasma technology in dye treatment

5.4.1. Experimental applications of cold plasma technology in dye treatment

The reactive radicals generated from cold plasma, such as ●OH, H_2O_2 and O_3, not only interact with the surface but also diffuse into the liquid phase, increasing the efficiency of liquid treatment. The treatment efficiency is highly dependent on the time and power output, with O_3 and ●OH radicals being the main reactants. These results demonstrate the potential of cold plasma for the treatment of wastewater containing organic pollutants, with outstanding advantages in energy efficiency and minimal environmental impact compared to conventional methods.

5.4.2. Process of application cold plasma technology in dye treatment

Figure 5.7 describes the layout of an experiment to treat a dye solution using the plasma jet system that we used in this research. The implementation process is divided into the following steps: (1) Start the plasma jet system and set the operating parameters; (2) Prepare the experimental equipment and samples; (3) Treat the MB solution using the plasma jet system; (4) Take samples and analyze the results.

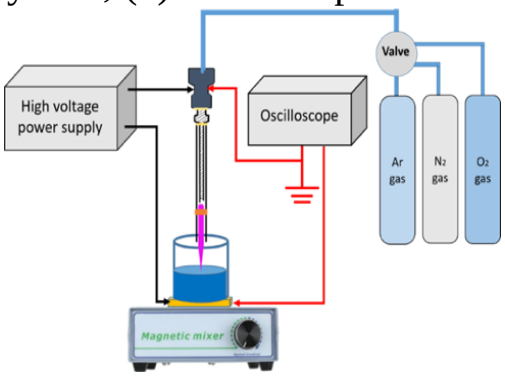

Figure 5.7. Setup of the plasma jet system used for the decomposition of the dye solution.

5.5. Survey and evaluation of dye decomposition efficiency

5.5.1. Decomposition rate of Methyl blue solution

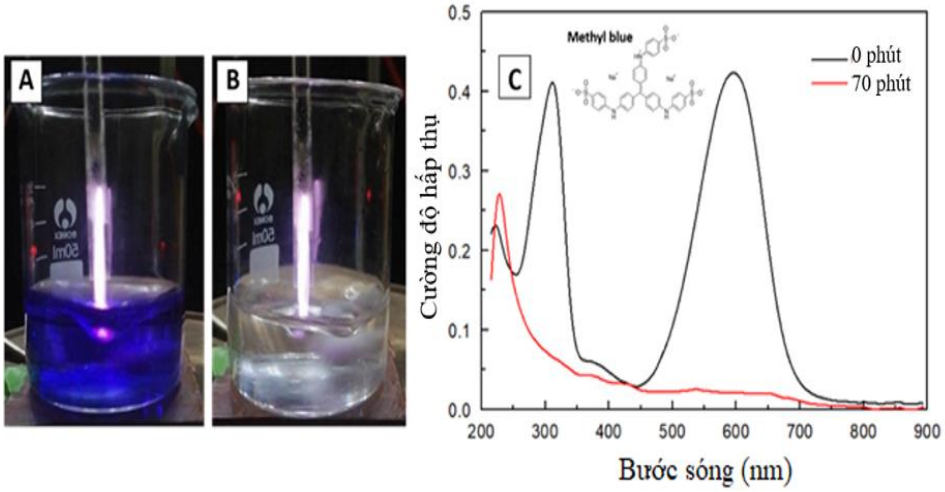

***Figure 5.8**. Methyl blue (MB) solution treated by Plasma jet system for 70 minutes: (A) Time 0 minutes; (B) Time 70 minutes; (C) Absorption spectrum of Methyl blue solution at 0 minutes and 70 minutes treated by Plasma jet.*

After 70 minutes of treatment with the plasma jet system, the solution had completely lost its color. The UV-VIS measurement results showed that the two characteristic absorption peaks at 310 nm and 600 nm of the initial solution had completely disappeared after the treatment process.

This proves that the cold plasma method is capable of completely and effectively decomposing the MB dye solution. We determined the decomposition efficiency (H_{ph}) of MB over time based on the following formula:

$$H_{ph} = \frac{C_0 - C_T}{C_O} X\ 100\%$$

C_0: concentration of Methyl Blue solution at initial time with t = 0.

C_t: concentration of Methyl Blue solution remaining after treatment time t minutes

The percentage decrease in dye concentration over time reflects treatment efficiency. In Figure 5.9, absorption peaks at 310 nm (aromatic rings) and 600 nm (C–O, C–N, C–C bonds) declined, indicating degradation. Two rates were calculated: kp_1 (aromatic degradation at 310 nm) and kp_2 (color loss at 600 nm).

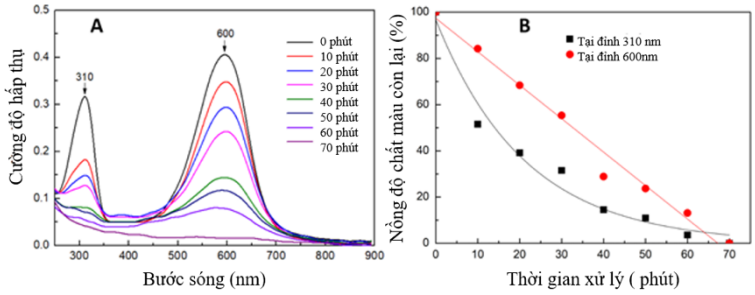

Figure 5.9. *(A) Absorption spectrum of Methyl Blue solution during treatment time from 0 to 70 minutes; (B) Percentage of remaining dye according to plasma treatment time.*

From the absorption spectra data in Figure 5.9A, we calculated and found that the decrease in absorption intensity at the 310 nm peak follows an exponential law, described by the following equation:

$$C_t = C_O e^{-k_{p1}.t}$$

Meanwhile, the intensity decrease at the 600 nm peak, representing the rate of color loss of the dye, shows a linear relationship and follows a first-order function law (equation (3). This first-order function law is described by the red line in Figure 5.9B, with the coefficient k_{p2}= 1,44 and coefficient of determination R^2 = 0,98.

$$\frac{C_t}{C_o} = -\left(\frac{k_{p2}}{C_o}\right)t + 1$$

5.5.2. Distance from plasma generator to solution surface (d)

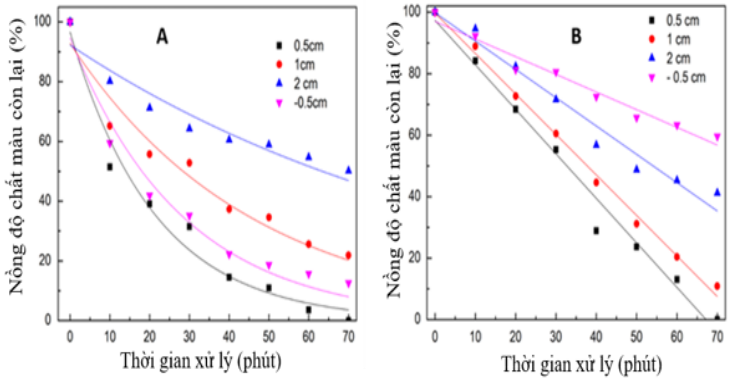

Figure 5.10. *Decomposition rate (A) at the 310 nm peak and (B) at the 600 nm peak when changing the irradiation distance d: 0.5 cm; 1 cm; 2 cm; - 0.5 cm.*

The plasma system was optimized at 12 V DC and 33 kHz for stable high-power operation. Key parameters—plasma-to-solution distance and gas flow rate—were adjusted to enhance decomposition. Table 5.1 shows that the optimal distance is 0.5 cm, yielding the highest kp_1 (degradation rate) and kp_2 (discoloration rate).

The distance d = 0.5cm achieved the highest efficiency due to the following factors: as the distance d increases, the contact area and penetration depth of the plasma beam into the solution are reduced, resulting in lower treatment efficiency.

5.5.3. Effect of air velocity

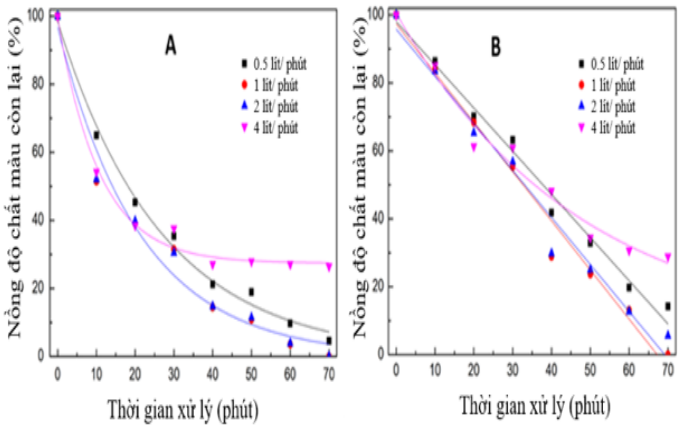

Figure 5.11. *Decomposition rate at (A) 310nm peak and (B) discoloration rate at 600 nm peak with gas flow rates: 0.5 l/min; 1 l/min; 2 l/min; 4 l/min.*

In this section, we investigated different gas flow rates to enhance the interaction between the plasma jet and the environment, thereby creating more powerful oxidizing radicals. From the survey results, the research team optimized the operating parameters of the plasma jet system to achieve the highest MB solution decomposition efficiency, including a distance of d=0.5cm and a gas flow rate of 1 l/min.

5.6. Mechanism of dye decomposition by cold plasma technology

The reactive substances and active free radicals generated during the discharge process that creates plasma are the main components involved in supporting the decomposition of pollutants in water and wastewater. However, in a typical plasma generation process, the chemical reactions are very complex and involve many active substances with different lifetimes and oxidation potentials. According to the above equations, the products generated are H_2O_2, •OH, $•O_2^-$ These three products are common agents for the decomposition of various dyes in other treatment methods such as photocatalysis, biology....

5.6.1. Effect of H_2O_2

H_2O_2 has an absorption peak at 225nm, so we can quantify the H_2O_2 produced over the Plasma irradiation time by using absorption spectrometry. Figure 5.12 shows the signal intensity value of H_2O_2 obtained after different irradiation times.

After 70 minutes of plasma irradiation, 24 mg/L of H_2O_2 was produced, but it did not affect Methyl Blue during plasma treatment. However, after irradiation stopped, H_2O_2 continued reacting, causing prolonged decolorization for over 5 hours.

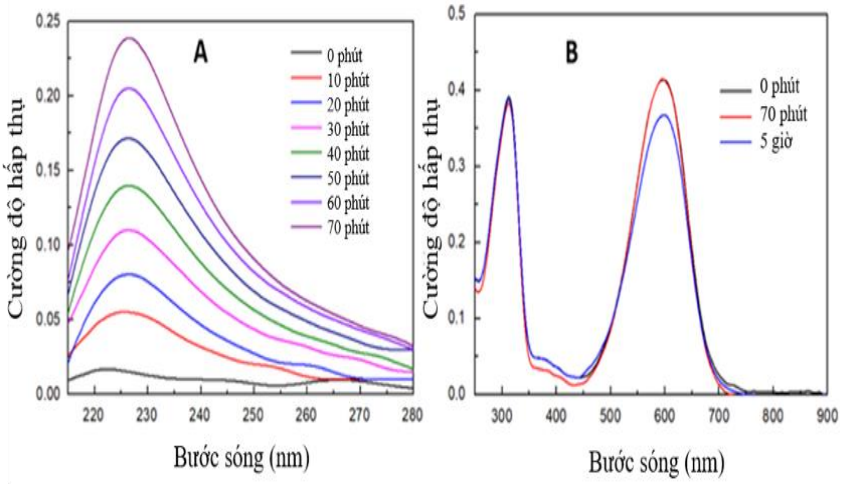

Figure 5.12. *(A) Absorption spectrum of H2O2 obtained after plasma irradiation into distilled water for 0 – 70 minutes; (B) Absorption spectrum of 30ppm Methyl Blue solution after 70 minutes, 5 hours of reaction with H2O2 solution at concentration of 24 mg/l.*

5.6.2. Effects of •OH (hydroxyl radicals)

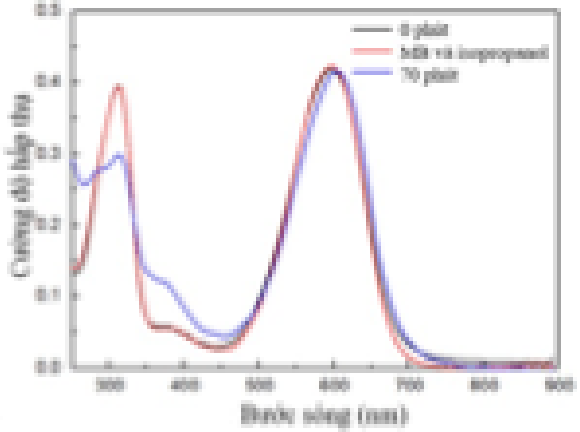

Figure 5.13. *Absorption spectrum of Methyl Blue solution decomposed by Plasma jet in the presence of isopropanol*

Here, we conducted an experiment to determine the effect of •OH on the decomposition process by adding 400 µl of isopropanol, a chemical that is very sensitive to hydroxyl radicals (when •OH radicals appear, this substance will react immediately) into the Methyl blue dye solution, then treating the solution mixture with Plasma. From Figure 5.13, we concluded that •OH is the main factor affecting the decomposition process of Methyl blue solution, especially affecting the overall discoloration process

5.6.3. Effects of •O2- (superoxide radical anion)

The results in Figure 5.14 show that: From there, the research team concluded that: •OH is a strong oxidizing radical and has the main influence in the decomposition process and completely determines the discoloration of Methyl blue solution; •O2- also plays a role in the decomposition process and discoloration of the solution; H2O2 has almost no role in decomposing Methyl blue dye solution during Plasma irradiation.

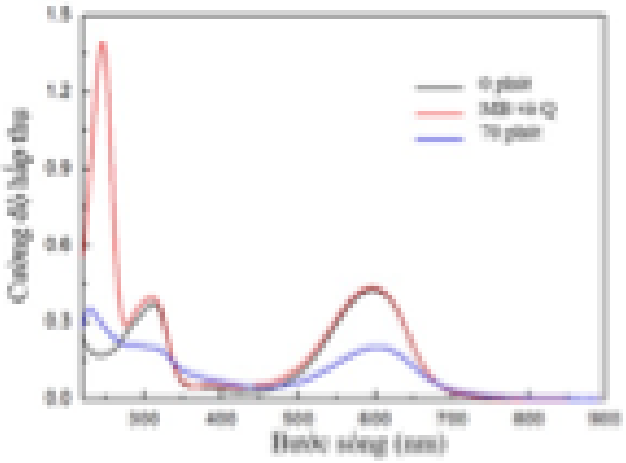

Figure 5.14. *Absorption spectrum of Methyl Blue solution decomposed by plasma jet in the presence of 1,4-benzoquinone.*

5.7. Chapter 5 Conclusion

This chapter showed that plasma jet enhances seed germination by improving surface wettability, increasing water absorption, and regulating GA_3 hormone. Germination coefficient rose 11× (after 12 h) and seedling length nearly 3× (after 96 h), with optimal plasma energy of 0.08 Wh/seed and NO at 20–95 ppm. In dye degradation, plasma treatment (12 V, 33 kHz, 1 L/min, 0.5 cm distance) decolorized 30 ppm Methyl Blue (20 ml) in 55 min, eliminating 310 nm and 600 nm peaks. The treated solution's COD dropped to 42.52 mg/L, within the QCVN 13-MT:2015/BTNMT threshold (75 mg/L). The research results in this chapter have been published in the journals Applied Sciences (IF 2.5), Materials Advances (IF 5.2), and Communications in Physics.

CONCLUSION

The thesis explores cold plasma applications in gold nanoparticle synthesis, SERS substrate fabrication, seed germination stimulation, and dye degradation.

1. Cold Plasma Jet System: Developed a high-voltage (2–6 kV), high-frequency (100 Hz–80 kHz) plasma jet with adjustable distance (0.2–2 cm) and gas flow (3.4–10 scm).
2. Gold Nanoparticles (AuNPs): Synthesized uniform, pure, stable AuNPs (~45 nm) in 5 minutes without chemical reducers. Optimal parameters: 0.4 cm nozzle distance, 1 l/min gas, 40 kHz frequency, 0.2 mM $HAuCl_4$, 10 ml volume.
3. SERS Substrate: Plasma and laser-treated SiO_2 improved hydrophilicity, surface texture, and AuNP deposition. Achieved 11× Raman intensity, 10× reuse, EF ~3×10^8 , and LOD of 10^{-12} M (R6G). Detected amoxicillin at 10^{-3}–10^{-9} M with $R^2 = 0.98$ and LOD 9×10^{-10} M.
4. Seed Germination: Plasma increased germination coefficient 11× (12 h) and seedling length 3× (96 h) at 0.08 Wh/seed and NO = 20–95 ppm. Plasma enhanced water uptake and regulated GA_3 hormone.

5. Dye Degradation: Plasma decomposed 30 ppm Methyl Blue (20 ml) in 55 min using 12 V DC, 33 kHz, 1 l/min gas, 0.5 cm distance. Post-treatment COD = 42.52 mg/L, meeting QCVN 13-MT:2015 standards. •OH was the key oxidant.

Cold plasma at atmospheric pressure is a fast, safe, effective, and eco-friendly technology with wide applications in materials science and agro-biomedicine.

LIST OF THE PUBLICATIONS RELATED TO THE DISSERTATION

1. **Le Thi Quynh Xuan**, Nguyen Nhat Linh, Dao Nguyen Thuan, 2021, Synthesis of stabilizer-free, homogeneous gold nanoparticles by cold atmospheric-pressure plasma jet and their optical sensing property. *Nanotechnology*, *33*(10), 105603.
2. **Le, T. Q. X.**, Nguyen Nhat Linh, Nguyen Thanh Tung, Eun Ha Choi, Nguyen Quang Liem, Nagendra Kumar Kaushik, Dao Nguyen Thuan, 2022, Effects of cold plasma treatment on physical modification and endogenous hormone regulation in enhancing seed germination and radicle growth of mung bean. *Applied Sciences*, 12(20), 10308.
3. **Le Thi Quynh Xuan**, Pham Thanh Binh, Nguyen Minh Thu, Nguyen Thu Loan, Nguyen Van Chuc, Dao Nguyen Thuan, 2024, A Novel Method for Rapid and High-Performance SERS Substrate Fabrication by Combination of Cold Plasma and Laser Treatment. *Nanomaterials*, *14*(21), 1689.
4. Nguyen Thi Huyen, Luong Chuc Quynh Ngan, **Le Thị Quynh Xuan**, Tran Ai Suong Suong, Cao Thi Thanh, Nguyen Van Tu, Pham Thanh Binh, Tran Ai Tan, Nguyen Viet Tuyen, Dao Tran Cao, Pham Van Hai, Vu Xuan Hoa, Nguyen Van Chuc, 2025, Reduced graphene oxide-carbon nanotubes nanocomposites-decorated porous silver nanodendrites for highly efficient SERS sensing. *Optical Materials*, 116935.
5. **Le Thi Quynh Xuan**, Tran Hong Quan, Trinh Thu Ha, Dao Nguyen Thuan, 2021, Removal of rhodamine B dye by plasma jet oxidation process. *Communications in Physics*, *31*(1), 95-102.
6. **Le Thi Quynh Xuan**, Nguyen Tuan Minh, Nguyen Van Chuc, Dao Nguyen Thuan, 2021, Enhancing surface energy of polycarbonate by atmospheric pressure plasma jet. *Vietnam Journal of Catalysis and Adsorption*, 10(1S), 293-296.
7. **Le Thi Quynh Xuan**, Tran Thi Thu Huong, 2020, Degradation of methyl blue by an approach using plasma jet processing, The 11th International Conference on Photonics & Applications.
8. **Le Thi Quynh Xuan,** Dao Nguyen Thuan, 2021, Degradation rhodamine b in solution by atmospheric pressure plasma jet, *The 10th International Workshop on Advanced Materials Science and Nanotechnology*.
9. **Le Thi Quynh Xuan**, Pham Thanh Binh, Nguyen Van Chuc, Dao Nguyen Thuan, 2024, A novel method for rapid and high-performance SERS substrate fabrication by combination of cold plasma and laser treatment, *The 11th International Workshop on Advanced Materials Science and Nanotechnology*.
10. Dao Nguyen Thuan, **Le Thi Quynh Xuan,** Process of manufacturing gold nanoparticles by plasma jet method, National Office of Intellectual Property, Application accepted 2021.